

Dusty Plasma Processes in Geophysics^{*)}

Sergey I. POPEL

Institute for Dynamics of Geospheres RAS, Leninsky pr. 38, bld. 1, Moscow 119334, Russia

(Received 13 August 2008 / Accepted 14 May 2009)

Review of dusty plasma phenomena in application to geophysical problems is presented. Possible observational manifestations of dusty ionospheric plasmas during high-speed meteor showers are described. A unified explanation of ionization properties of the polar mesosphere under summer conditions is given. Dusty plasma processes are also considered in application to active geophysical rocket experiments which involve release of some gaseous substance in near-Earth space, the origin of the primary Earth's crust, hydrosphere, and atmosphere, and global electromagnetic Schumann resonances.

© 2009 The Japan Society of Plasma Science and Nuclear Fusion Research

Keywords: dusty ionosphere, polar mesosphere, dust acoustic wave, Schumann resonance, active geophysical experiment

DOI: 10.1585/pfr.4.031

1. Introduction

Processes taking place in plasmas containing charged nano- and microscale particles have been the subject of extensive studies in recent years [1–3]. Systems of this kind are generally called dusty (or complex) plasmas. In nature, charged dust grains are present in planetary magnetospheres and ionospheres, atmospheres of comets, and interstellar medium [4–6]. In the Earth's troposphere, dust from natural and anthropogenic sources is present at different altitudes [7]. The dust can ascend to the stratosphere and ionosphere in the course of violent volcanic eruptions, rocket launchings, and high-altitude flights and also as a result of convective and synoptic processes in the atmosphere [5, 8–10]. Frequently, dust grains strongly affect, and may even determine, environmental conditions.

Charged grains can lead to many physical effects having unique observable features [4, 5, 11–14]. The latter include ionospheric phenomena such as noctilucent clouds (NLC) and polar mesosphere summer echoes (PMSE), where dust grains result, in particular, from condensation of water vapor (see, e.g., [5]). The Earth's ionosphere can also become contaminated with dust particles as a result of bombardment by meteor showers. Ablation of the meteors at altitudes of 80 to 120 km in the lower ionosphere produces supersaturated vapors of metals such as sodium, calcium, magnesium, etc. [15], which then condense into small grains with characteristic sizes of several nanometers to a few tenths of a micrometer. In the ionosphere there can exist also larger, primary grains consisting of meteors that have been slowed down in the atmosphere, as well as fragments of larger meteors or of meteors that have not been completely burned out. In the ionosphere, dust grains are charged due to photoelectric effect and the absorption of

electrons and ions from the surrounding plasma. Therefore, the plasma of the dusty ionosphere can be considered as a dusty (complex) plasma [5, 13]. Dusty plasma in the ionosphere can also be formed [17] during active geophysical rocket experiments, which, e.g., use the scheme of the experiments “Fluxus” [18, 19] and/or “North Star” [20] and involve the release of some gaseous substance in near-Earth space. Dusty plasmas present even in the lower atmosphere. For one thing, this concerns the plasma of lightning discharges containing nano- and microscale particles and can be important from the viewpoint of the properties of electromagnetic oscillations in the Schumann cavity [16].

Understanding of the processes taking place in dusty plasmas has been significantly improved owing to laboratory investigations conducted since the mid-1990s (see, e.g., [1–3]). This motivates the application of methods developed in studies of dusty plasmas to Earth's environments. Interest in the dusty plasma research is often associated with the fact that the processes of dust grain charging are far from equilibrium, so that the anomalous dissipation, which, by its very nature, originates from the dust particle charging process, can play a decisive role [21]. Other specific features of dusty plasmas distinguishing them from other plasma systems are an appearance of new linear wave modes, e.g., dust acoustic (DA) mode [22], a modification of the character of nonlinear processes, an existence of new types of nonlinear wave structures, e.g., shocks [23] associated with the above mentioned anomalous dissipation. The purpose of this paper is to review such geophysical plasma phenomena where the processes inherent in dusty plasmas are important.

In Sec. 2, experiments measuring radio emission from the dusty ionosphere are described. In Sec. 3, a mechanism for generating low-frequency (LF) ionospheric noise, which is associated with the modulational excitation of

author's e-mail: s.i.popel@mtu-net.ru

^{*)} This article is based on the invited talk at the 14th International Congress on Plasma Physics (ICCP2008).

DA perturbations during intensive meteor showers, is considered. In Sec. 4, excitation of infrasonic and acoustic gravitational waves by DA perturbations and their possible observable consequences are investigated. In Sec. 5, dusty plasma effects associated with NLC and PMSE are described. In Sec. 6 dusty plasma phenomena in active geophysical rocket experiments, primary Earth, and Schumann resonances are discussed. A summary is given in Sec. 7.

2. Radio Noise from Dusty Ionosphere

Here, we describe the results of ground-based experiments carried out from 1999 to 2000 and in 2003 [24, 25] measuring radio emission from the dusty ionosphere. These measurements allowed the authors to identify the characteristic features of the radio emission spectra typical for dusty ionospheric plasmas. The equipment and software specifically developed for this purpose make it possible to measure and study ionospheric radio noise with a registration characteristic time of 0.005 s. The equipment includes, in particular, a modulation radiometer at $\lambda = 2$ m with a low-noise input amplifier (characterized by a noise temperature $T_{\text{noise}} \sim 120$ K) and an antenna (in the meter band) system with a mobile measuring complex. The typical Fourier spectra of ionospheric radio noise measured on August 12, 1999 are given in Fig. 1.

Studies of the Fourier spectra of the ionospheric radio noise indicated that maxima (“dust” lines) are present in the spectra in addition to the known types of noise. It is

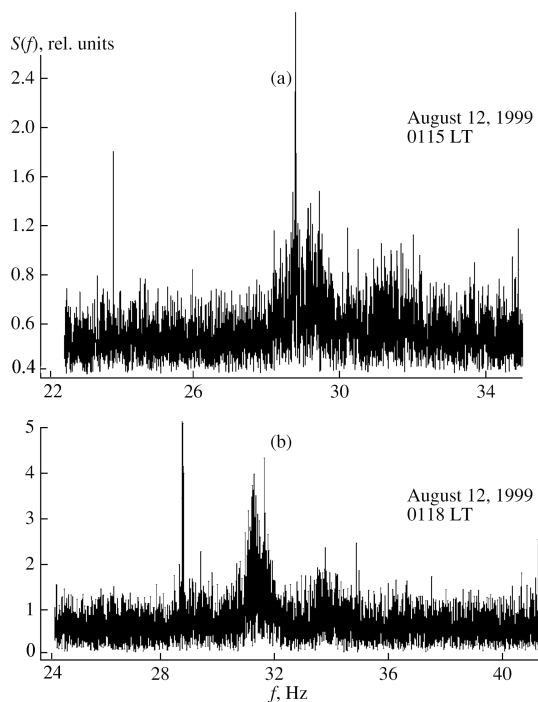


Fig. 1 Parts of the Fourier spectral band (August 12, 1999) with the dust line and satellites in the region 26–33 Hz for (a) $t = 0115$ LT and (b) $t = 0118$ LT [25].

thus possible to conclude that a dusty-plasma component, which manifests itself in the frequency band 12–50 Hz, exists in the ionosphere during the meteor showers. According to Musatenko *et al.* [25], this frequency band can be attributed to either the emission from the ionospheric layers where the density of the charged particles is considerably enhanced during the meteoric showers, or to the modulation of the ionospheric emission.

(1) The dust line is registered during the maxima of meteor showers with high-speed ($V \sim 60$ –70 km/s) entry into the Earth’s atmosphere: Perseids, Orionids, and Leonids of the June meteor shower. The line is also registered during low-speed meteor showers, but it is weak and has a short lifetime, such as in the Geminids-2000 meteor shower.

(2) The line can be composed of isolated spectral density peaks. The peak frequency and amplitude can vary both within and outside the group. Satellites appear in the latter case. Instantaneous peak frequencies can differ considerably from the average values.

(3) The line manifests itself in the spectra in two ways: (a) the line starts at 40–50 Hz and shifts to 28–30 Hz during 10–15 min, (b) the line starts at 20–26 Hz and fluctuates around this level.

(4) The averaged line profiles can be easily obtained only for individual time intervals since the line is composed of isolated groups of oscillations. These profiles are rarely symmetrical and they often break sharply near the LF end of the spectrum. The line width without satellites is 1.5–3.0 Hz and can sometimes reach 4.0 Hz. The line is sometimes separated into two to three independent weaker components. The line shape can sometimes be approximated by the Gaussian. Line satellites, usually up to 3–5 Hz, often appear on the high-frequency (HF) side.

(5) The line appeared most often at night.

(6) The line is registered at a moderate level of solar activity ($F10.7 \sim 130$ –160 sfu) and at low or moderate geomagnetic activity ($\Sigma Kp = 4$ –20, indicating that the intensity of particle precipitation from the magnetosphere into the ionosphere is low). Under such conditions, the line frequency is highly variable (up to 30 Hz). At a higher level of geomagnetic activity, the line frequency varied within 5–6 Hz.

(7) The lowest frequencies in the spectra of the radio noise fluctuations are about 0.01–0.1 s⁻¹ (see Fig. 2, which shows the lower-frequency part of a spectrum of radio noise fluctuations in the Earth’s ionosphere during a Perseid meteor shower [24, 26]). The distinguishing feature of the studies carried out in Refs. [24, 25] is the use of an accurate and precise procedure for singling out disturbances of the radio noise spectra.

3. Excitation of LF Perturbations

Several mechanisms that might be responsible for the origin of dust lines were proposed, in particular, they were

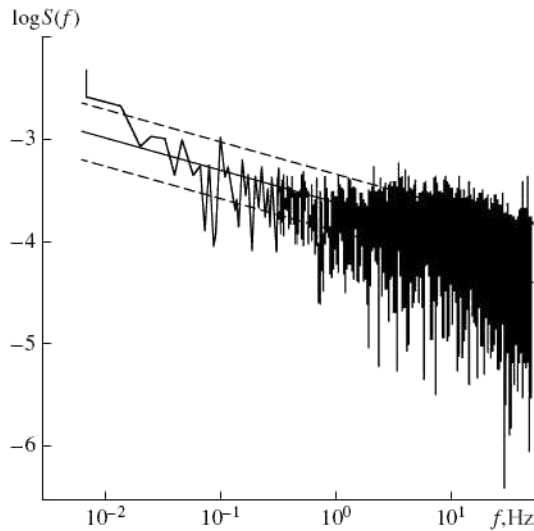


Fig. 2 LF part of a typical spectrum of the radio noise fluctuations in the ionosphere according to the data from measurements on August 11-12, 1999 during the Perseid meteor shower [24, 26].

interpreted as disturbances, as Schumann resonant harmonics, as the result of nonlinear nondusty processes in the ionospheric F region, or of nonlinear modulations in the entrance of the radiometer, or of the scattering of radiation by turbulent pulsations in the troposphere or ionosphere [25]. Yet, none of them can explain why the lines were observed exactly during the high-speed meteor fluxes mentioned above.

The frequency range of 12-50 Hz is typical of a DA mode. The generation of radio noise fluctuations can be attributed to the presence of dust grains condensed from supersaturated vapors of substances and materials that come into the ionosphere as a result of the ablation of meteors [27]. Note that, since DA waves are longitudinal, they exist only in a plasma and cannot reach the Earth's surface, where the measurement equipment [24, 25] was installed. Therefore, only electromagnetic waves can be observed at the Earth's surface.

The LF (12-50 Hz) emission corresponds to wavelengths of electromagnetic waves exceeding or of order the Earth's radius. Such wavelengths could not be observed in the experiments [24, 25]. Hence, the presence of the LF component in the electromagnetic wave spectrum is an indication of modulation of the electromagnetic waves escaping from the ionosphere. The wave modulation can result, e.g., from the modulational interaction [28] between the electromagnetic and DA waves. The dispersion relation of the DA waves in the ionospheric plasma at altitudes of 80 to 120 km is

$$\omega_s(k) = \sqrt{\frac{\omega_d^2}{b(k)} - \left(\frac{\nu_{dn}}{2}\right)^2} - i\frac{\nu_{dn}}{2}, \quad (1)$$

where $\omega_d^2 = 4\pi n_{d0} q_{d0}^2 / m_d$ is the dust plasma fre-

quency, n_d is the number density of dust grains, q_d is the dust particle charge, m_d is the dust particle mass, $\nu_{dn} = (4/3)\pi a^2 \sqrt{8T_{n0}/\pi m_n n_n} (m_n/m_d)$ is the effective dust-neutral collision frequency, n_n , m_n , T_{n0} are the number density, the mass, and the temperature of neutrals, respectively, and a is the dust particle size. The subscript 0 corresponds to unperturbed values. In the case of positive dust charges we obtain [26]

$$b(k) = 1 + \frac{1}{k^2 \lambda_{De}^2} \left(1 + \frac{\bar{\nu}_e}{\nu_{ch}}\right), \quad (2)$$

and for $q_d < 0$ we have

$$b(k) = 1 + \frac{\tau \nu_{ch} + (1 + \tau) \bar{\nu}_e}{\tau \nu_{ch} k^2 \lambda_{De}^2} + \frac{1}{k^2 \lambda_{Di}^2}, \quad (3)$$

where $\lambda_{De(i)} = \sqrt{T_{e(i)}/4\pi n_{e(i)} e^2}$ is the electron (ion) Debye length, $-e$ is the electron charge, $T_{e(i)}$, $n_{e(i)}$, and $m_{e(i)}$ are the electron (ion) temperature, number density, and mass, respectively, $\tau = T_{i0}/T_{e0}$, $\bar{\nu}_e$ is the electron-dust collision frequency, $\nu_{ch} = -[\partial I^{eq}(q_d)/\partial q_d]_{q_d=q_{d0}}$ is the characteristic dust particle charging frequency, and $I^{eq}(q_d)$ is the total (including electron, ion, and for $q_d > 0$ photoelectric) microscopic current on the dust particle [26].

During the Perseid, Orionid, Leonid, and Geminid meteor showers, the LF background radio noise fluctuations can be substantially enhanced by the modulational interaction of the electromagnetic waves in the ionospheric plasma when dusts are present. It is suggested that the observed radio noise fluctuations (dust lines) stem directly from the modulational instability. Under this circumstance, the fluctuations are the LF virtual electrostatic fields (which are, in general, not propagating fields) that are excited by the HF fields (here the electromagnetic waves) [28]. The peaks that appear against the background of LF virtual fields can be associated with DA waves, which obey a given dispersion relation (see Fig. 3) [28], and can thus correspond to the spectral density peaks [25] characterizing the structure of the dust lines.

The main conclusions concerning the development of the modulational instability of electromagnetic waves in the lower dusty ionosphere are the following [26]. Perturbations on the ion acoustic time scales are suppressed there by ambipolar diffusion. Thus the modulational instability gives rise to LF electromagnetic fields that can be associated with modulation by the DA mode. The modulational instability is caused by Joule heating, the ponderomotive force, as well as processes related to the charging of dust grains and their dynamics. For $q_{d0} < 0$ [29] (e.g., at night time when photo-emission is absent), the modulationally excited LF (dust acoustic) perturbation frequency Ω and the maximum growth rate of the modulational instability Γ are given by the expression [26]

$$\Omega \sim \Gamma \sim \left(\frac{\nu_e c^2}{\chi_e}\right)^{1/2} \frac{\omega_{pe}^6}{\nu_e \omega_0^5} \frac{|E_0|^2}{4\pi n_{e0} T_{e0}}. \quad (4)$$

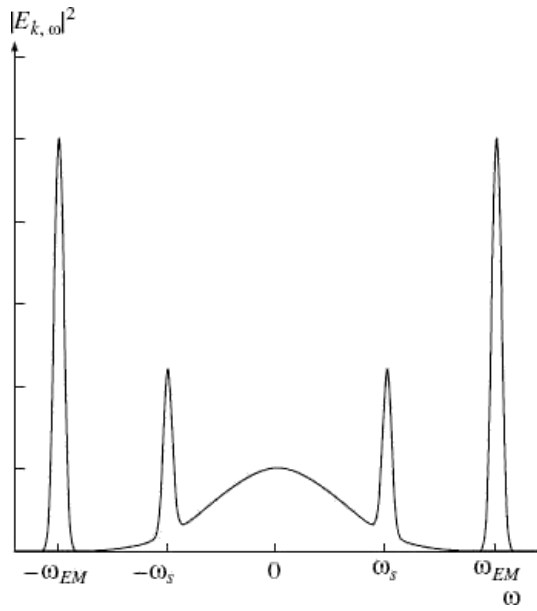


Fig. 3 Spectrum of the electromagnetic waves with the dispersion $\omega_{EM}(k)$, the LF DA waves with the dispersion $\omega_s(k)$, and the virtual LF fields.

For $q_{d0} > 0$ [30] and $\Omega \gg \omega_{\chi e} \gg C_{Sd}K$, we have [26]

$$\Omega \sim \Gamma \sim \left[\nu_e \omega_{pe}^2 \left(\frac{\omega_{pe} C_{Sd}}{\omega_0 c} \right)^2 \frac{|E_0|^2}{4\pi n_{e0} T_{e0}} \right]^{1/3}, \quad (5)$$

and in the case $q_{d0} > 0$ and $\omega_{\chi e} \gg \Omega \gg C_{Sd}K$ the perturbation frequency and the growth rate are [26]

$$\Omega \sim \Gamma \sim \left(\omega_0 \frac{C_{Sd}^2 \omega_{pe}^4}{\chi_e \omega_0^4} \frac{|E_0|^2}{4\pi n_{e0} T_{e0}} \right)^{1/2}. \quad (6)$$

Here, E_0 and ω_0 are the amplitude and the frequency of the electromagnetic pump wave, $\omega_{\chi e} = \chi_e K^2$, $K = |\mathbf{K}|$ is the length of the wavevector of the modulational perturbations, $\chi_e = 3.16 T_e / m_e \nu_e$ is electron thermal conductivity coefficient, ν_e is the electron collision frequency, $\omega_{pe} = \sqrt{4\pi n_e e^2 / m_e}$ is the electron Langmuir frequency, c is the speed of light, $C_{Sd} = |q_{d0} / e| \sqrt{n_d T_e / n_e m_d}$ is the DA speed.

Clearly, the modulational instability can develop only when its growth rate appreciably exceeds the damping rate $\nu_{dn}/2$ (see the dispersion relation (1)) of the DA waves. For a wide range of ionospheric parameters, this damping rate is about $\nu_{dn} \sim 0.01-0.1 \text{ s}^{-1}$. It is this value that determines the threshold for the modulational instability of electromagnetic waves in a plasma. This instability threshold agrees well with that deduced from observations, $\Omega > \nu_{dn}/2$, as confirmed by the data in Fig. 2, which shows representative spectra of the radio noise fluctuations in the Earth's ionosphere during a Perseid meteor shower.

Thus, the mechanism for generating LF ionospheric noise [25] can be summarized as follows. During Perseid, Orionid, Leonid, and Geminid meteor showers, the

meteors are ablated at altitudes of 80-120 km, depending on their sizes and initial velocities. The result of the ablation is production of supersaturated vapors of metals such as sodium, calcium, magnesium, etc., which then condense into nanometer-to-micrometer-sized secondary (dust) grains of cosmic origin. The grains can acquire electric charge because of unbalanced electron and ion currents to them and because of the photo-emission resulting from solar radiation. As electromagnetic waves propagate in the dusty lower ionosphere, modulational interaction can excite LF electrostatic perturbations at characteristic frequencies close to that of the DA waves. As a result the electromagnetic waves become modulated. It is the LF component of the modulated wave against the ionospheric noise background that is recorded at the Earth's surface [25].

We emphasize that the modulational excitation of LF electrostatic perturbations associated with the DA waves is possible only when dust grains are present in the ionosphere. As it has been mentioned, the dust grains appear during the meteor showers. Thus the mechanism described above is inherent in the time periods of high-speed meteor showers.

4. Other Manifestations of DA Waves

Here, we discuss other manifestations of DA perturbations excited by the modulational instability of electromagnetic waves in the ionosphere. The frequency of the DA waves lies in the infrasonic range, from several hundredths of a hertz to several tens of hertz. This points to a possibility of excitation of infrasonic waves by the DA perturbations interacting with neutrals [31].

The upper frequency of the infrasonic range is generally thought to be 16-25 Hz. The lower frequency of the range is uncertain. Infrasonic waves occur during earthquakes, underwater and underground explosions, storms and hurricanes, tsunamis, volcanic eruptions, and so on [32–36]. Among the main anthropogenic sources of infrasonic waves are chemical and nuclear explosions and also high-power engine (in particular, rail and motor transport, aviation, rockets, and great industry). Since infrasonic waves are weakly absorbed in air, as well as in water and within the Earth's crust, they propagate over very long distances and can serve as indicators of cataclysmic events, such as storms, hurricanes, tsunamis, etc.

For a fixed wavelength of the modulation, the maximum amplitude of the electrostatic potential φ in the DA perturbation excited due to the modulational instability is

$$\varphi_0 \approx 8\pi q_{d0} \frac{n_{e0}}{K^2} \left(\frac{C_{Sd}}{c} \right)^2 \frac{\Omega}{\omega_0} \frac{|E_0|^2}{4\pi n_{e0} T_{e0}}. \quad (7)$$

Dust-neutral collisions result in the appearance of forced or driven oscillations (at the same frequency and wave vector as that of the DA perturbation) of the neutrals. The forced neutral particle oscillation is a source for infrasonic waves. The evolution of the latter can be described by the wave

equation with a forcing term on the right-hand side (see Sec. 75 of Ref. [37]),

$$\frac{1}{C_S^2} \frac{\partial^2 P_{n1}}{\partial t^2} - \Delta P_{n1} = \rho_0 \nabla \cdot (\mathbf{v}_n \cdot \nabla \mathbf{v}_n), \quad (8)$$

where \mathbf{v}_n is the speed acquired by the neutrals due to their interaction with DA perturbations, ρ_0 and C_S are the background mass density of neutrals and the acoustic speed at the corresponding altitude.

Since the height of a dust cloud is of the order of 1 km [38] (a value that is much less than the characteristic spatial scale, 7.5 km, on which the atmospheric air density varies), we can solve Eq. (8) by assuming that ρ_0 is independent of altitude. Thus Eq. (8) can be treated as a retarded potential equation and solved by standard methods [37].

The estimate of the maximum amplitude of the infrasonic waves near the Earth's surface, obtained on the basis of Eq. (8), gives:

$$P_{n1,\max} \sim \frac{\rho_0 V_1}{4\pi h_0} \frac{\delta K}{K} \left(\frac{\varphi_0 n_{d0} q_{d0}}{P_{n0}} \right)^2 \times \frac{\exp(m_n g h_0 / 2T_{n0})}{\Omega^{-2} + \nu_{dn}^{-2}}, \quad (9)$$

where V_1 is the volume of the dust cloud, P_{n0} is the background pressure at the altitudes of the dust cloud, δK is the characteristic wave vector of infrasonic wave (determined by the sum of two wave vectors of the DA perturbations), h_0 is the altitude of dust layer localization.

For the characteristic parameters of the dusty plasma of the lower ionosphere [39] (namely, a neutral temperature of $T_{n0} = 130\text{--}200$ K, a neutral density of $n_n = 10^{12}\text{--}10^{15}$ cm⁻³, a characteristic grain size of $a \sim 1\text{--}10^3$ nm, a dust density of $n_d = 10\text{--}10^3$ cm⁻³, an electron density of $n_e \sim 10^4\text{--}10^5$ cm⁻³, and an ion density of $n_i \sim 10^4\text{--}10^5$ cm⁻³), the maximum pressure amplitude $P_{n1,\max}$ can be about several pascals. Figure 4 displays the amplitude–frequency characteristics showing how infrasonic waves from various sources (in particular, large and small explosions, Rayleigh waves during earthquakes, magnetic substorms, hurricanes, tornadoes, supersonic aircraft, microbaroms and thunderstorms, mountain wave activity, and so on) are distributed near the Earth's surface. Curve 7 characterizes infrasonic waves originating from DA waves in the Earth's lower ionosphere during meteor showers. This curve was calculated for the following parameters: the altitude at which the dust cloud is localized is about $h \approx 90$ km, the characteristic height of the cloud is of the order of 1 km, the horizontal dimension of the cloud is 10 km, the size of the dust grains in the cloud is about $a \approx 25$ nm, the dust density is about $n_d \approx 10^2$ cm⁻³, the electron density is $n_e \approx 10^5$ cm⁻³, and the neutral temperature is $T_{n0} = 140$ K. We can see that, in the frequency range from several tenths of a hertz to several tens of hertz, the generation of infrasonic waves by DA perturbations during meteor fluxes can be the most important

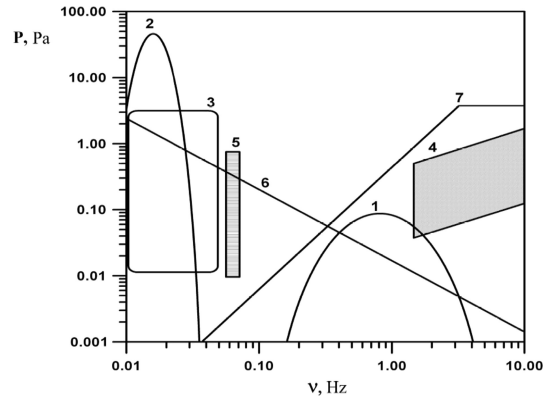


Fig. 4 Amplitude–frequency characteristics showing how infrasonic waves from various sources are distributed near the Earth's surface: (1) the region of infrasonic perturbations originating from small explosions; (2) the region of infrasonic perturbations originating from large explosions; (3) the region of infrasonic waves from Rayleigh waves during earthquakes, magnetic substorms, hurricanes, tornadoes, and mountain wave activity; (4) the region of infrasonic waves generated by supersonic aircraft and thunderstorms; (5) the region of infrasonic waves from microbaroms; (6) the local turbulent noise region; and (7) the region of infrasonic waves excited by a DA mode during meteor fluxes.

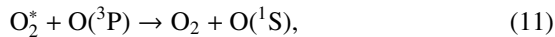
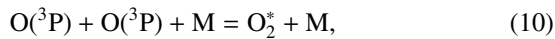
process whereby infrasonic waves arise near the Earth's surface.

DA perturbations can also serve as a source of acoustic gravitational waves (AGWs), which have wavelengths greater than, or of the order of, 1 km and frequencies in the infrasonic range. Here, we consider the main effects [31] by which AGWs show up during meteor fluxes and which can be observed from the Earth's surface.

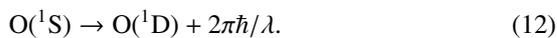
The AGWs are convectively unstable at altitudes of 110–120 km. Due to the instability, these waves can grow in amplitude. Moreover, the only growing waves are those that pass through the convective instability zone. When the amplitudes of the AGWs generated by DA perturbations during meteor fluxes grow to values of the order of the background pressure of the surrounding medium, the linear wave process becomes nonlinear. The competition between the nonlinear effects and the effects of dispersive spreading can give rise to steady localized nonlinear vortex structures [40]. Note that, at altitudes of 110–120 km, the dust density is low, so the dust acoustic perturbations generated there by the modulational instability are unlikely to grow at a rate much faster than the growth rate of the AGWs, $\gamma_a \approx 0.2$ s⁻¹ [31]. In analogy with conventional acoustic waves, the generation of AGWs by dust acoustic perturbations is a far slower process than the development of the modulational instability. Consequently, whereas the amplitude of the conventional acoustic wave is determined by the amplitude of the DA perturbation, the convective instability at altitudes of 110–120 km causes an AGW to

evolve in a different way, specifically, the most important processes governing the amplitude of acoustic gravitational perturbations are nonlinear processes that give rise to acoustic gravitational vortices, while the modulational instability serves merely to trigger acoustic gravitational perturbations.

The vortex structures can increase the intensity of green nightglow. At altitudes of 80-120 km, the green line is excited by the two-step Barth–Hildebrandt mechanism, consisting of two reactions [41],



followed by the emission of the oxygen green line ($\lambda = 557.7$ nm) in the reaction



Here, $\text{O}(^3\text{P})$ is the atomic oxygen in the ground state, O_2^* is the molecular oxygen in an excited state, M is an arbitrary neutral molecule, and $\text{O}(^1\text{S})$ and $\text{O}(^1\text{D})$ are the atomic oxygen in excited states.

The intensity of the emitted green line is proportional to the third power of the atomic oxygen density [40]. The density of atomic oxygen can vary because of the presence of localized nonlinear vortex structures or dust Rayleigh-Taylor instabilities [40, 42, 43]. The appearance of such dust-driven vortices and instabilities can result in a convective overturn of oxygen in vertical direction and thus in an enhancement of the atomic oxygen density at 110-120 km. For the characteristic conditions of the normal atmosphere at altitudes of about 110 km we obtain [31]

$$\frac{\Delta I}{I_s} \sim (1 + 10^{-2}u)^3 - 1, \quad (13)$$

where I_s is the mean seasonal green emission intensity and $\Delta I = I_{\text{Ob}} - I_s$, with I_{Ob} being the observed green line intensity, u is the speed of the steady waves propagating horizontally. For the characteristic velocities u ($u \leq 130$ m/s), the ratio $\Delta I/I_s$ can be about 10%, a level detectable on the Earth's surface [41].

Thus excitation of infrasonic waves by the modulationally excited DA perturbations can result in two observational manifestations: (a) direct observation of infrasonic acoustic waves at the Earth's surface, and (b) amplification of the intensity of the green emission at 557.7 nm from the region of the lower ionosphere at the altitudes of 110 to 120 km.

5. Polar Mesospheric Dust Clouds

One important feature of the polar mesosphere under summer conditions is the presence of dust layers (very thin on the atmospheric scale) located at altitudes of 80 to 85 km (NLC) or 85 to 95 km (PMSE). NLC consist of submicron-sized particles. Their vertical optical thicknesses are much less than unity, but they can be seen by

the naked eye at sunset, whereas PMSE (apparently consisting of charged nanoscale particles) cannot be observed by optical methods and manifest themselves by strong radio reflections observed with radars at frequencies between 50 and 1000 MHz [44]. Strong correlation between observations of NLC and PMSE suggests that they have a common origin. In the literature, NLC and PMSE are frequently grouped together under the common term polar mesospheric clouds (PMC) [11].

The formation of NLC and PMSE takes place in the polar atmosphere at mesospheric altitudes (80 to 95 km) between the end of May and the end of August. In this period, the ambient air temperature in the polar mesosphere falls below 150 K [11], and water vapor supersaturates. This leads to conditions favoring the growth of dust grains. The dominant nucleation mechanism appears to be the condensation of water molecules on nanoscale grains, which are always present at mesospheric altitudes. The characteristic grain size is a few nanometers [5, 39], and their density typically is 10 to 1000 cm^{-3} . Particle nucleation conditions are satisfied at altitudes between 78 and 92 km, where water vapor is supersaturated. Note that it is in this altitude range where NLC and PMSE are observed.

Microscopic currents of electrons and ions in the ambient plasma and their recombination on the surface of a dust particle result in its charging. This leads to a considerable decrease in positive-ion and electron densities in the regions occupied by NLC and PMSE. Effects due to solar radiation may lead to much more complicated behavior of charged species in dusty ionospheric plasmas, depending on the photoelectric properties of dust particles, their density, and grain size.

A systematic analysis of sounding rocket flight experimental results concerning the behavior of charged species in the polar mesosphere under summer conditions shows that five trends can be identified [5, 44–46]:

- (a) considerable dips (“bite-outs”) in both electron and positive-ion densities at altitudes between 80 and 85 km;
- (b) considerable decrease in the electron density without any significant change in the density or composition of the positive-ion subsystem;
- (c) a considerable increase in electron density in the region occupied by NLC while no measurements of ion densities were performed;
- (d) a considerable increase in the density of positive ions accompanied by a dip in electron density;
- (e) no appreciable change in the electron and positive-ion densities while strong radio reflections were observed in the mesosphere (at altitudes between 80 and 85 km) in radar frequency bands of 50 to 1000 MHz.

These results can be explained by the presence of dust particles in the middle atmosphere. For this purpose a theoretical model [5] has been developed which provides a self-consistent description of spatiotemporal variations of the plasma composition in the polar mesosphere under summer conditions and formation of NLC and PMSE

and takes into account sedimentation of dust grains in the middle atmosphere, their growth in a supersaturated water vapor, and dust particle charging processes, allowing for variations of the ion subsystem composition in the polar mesosphere and photoelectric emission. Microscopic electron and ion currents incident on the grains are calculated by using the orbit-limited probe model (see, e.g., [5, 47]), in which the cross sections for collisions of electrons and ions with a charged grain are determined by angular-momentum and energy conservation laws.

Discuss the results obtained by applying the above theoretical model to the polar ionosphere at 80 to 95 km under summer conditions. Our discussion is focused [5] on the possibility of explaining the most important experimental data concerning behavior of charged species in a dusty ionosphere. Figure 5 shows the evolution of vertical grain size distribution and the mean grain size versus time and altitude. The figure clearly demonstrates the growth of sedimenting particles and the formation of a layer of dust grains of characteristic diameter $2a \approx 0.5 \mu\text{m}$ at altitudes of about 80 km over a few hours, with a grain density of $n_d \approx 10\text{-}1000 \text{ cm}^{-3}$. The grain residence time in the mesosphere increases in the presence of upward air flow, and the characteristic grain diameter increases accordingly. The inset illustrates the effect of upward air flow on the characteristics of a single grain of radius $r_0 = 3 \text{ nm}$ initially located at $h_0 = 85 \text{ km}$. The vertical location h_d and radius r_d of the grain are plotted versus time. The vertical wind speed v_{wind} was set equal to 10 cm/s , which is close

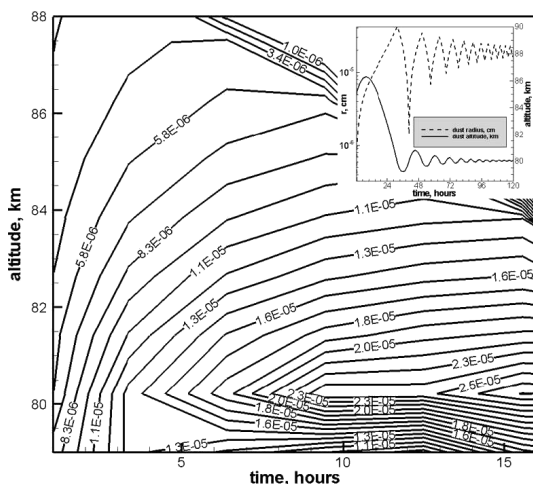


Fig. 5 Mean dust-grain size (shown at curves in centimeters) versus time and altitude as a characteristic of dust sedimentation in the polar mesosphere under summer conditions. Formation of a layer of particles $0.3\text{-}0.5 \mu\text{m}$ in diameter at altitudes of about 80 km over a time period of about 10 h is demonstrated. The inset shows typical altitude (solid curve) and radius (dashed curve) of a dust grain versus time as characteristics of the effect of upward air flow on particle motion. Vertical air velocity is 10 cm/s .

in order of magnitude to wind speeds observed in the polar mesosphere under summer conditions. With time elapsed, $r_d \rightarrow r_\infty \approx 200 \text{ nm}$ and $h_d \rightarrow h_\infty = 80 \text{ km}$. The values of r_∞ and h_∞ are independent of the initial values h_0 and r_0 , being determined only by v_{wind} . Therefore, when the upward velocity of air motion in the mesosphere is not zero, the grains leaving a dust cloud rapidly evaporate, their size decreases, and upward air motion brings them back into the mesosphere, where they grow and settle again. As a result, a sharp lower boundary of the dust cloud appears at the altitude h_b determined by the condition

$$\Phi_{\text{H}_2\text{O}}(h_b) = P_{\text{H}_2\text{O}}(h_b)/P_{\text{sat}}(h_b) = 1, \quad (14)$$

where $\Phi_{\text{H}_2\text{O}}$ is the degree of saturation of water vapor, $P_{\text{H}_2\text{O}}$ is the partial pressure of water vapor, P_{sat} is the pressure of saturated water vapor. For a grain of radius $r_0 = 3 \text{ nm}$, the minimum upward velocity required to bring a grain back into the mesosphere is relatively low, and can easily be reached under summer conditions in the polar mesosphere by virtue of the existence of the circumpolar vortex. Thus, the sedimentation and growth of nanoscale grains in the mesosphere lead to the development of a narrow layer of submicron-sized particles at altitudes of 80 to 85 km, i.e., where NLC are observed.

The presence of submicron-sized particles in the mesosphere has a strong effect on plasma characteristics (depending on photoelectric properties of dust-grain material). This effect is illustrated in Fig. 6 by spatiotemporal variations of mesospheric ion and electron densities in the presence of a layer of dust grains characterized by different values of the work function. The right panels correspond to pure ice dust particles. In this case, since there is no photoelectric emission, the dust particles are negatively charged and both ion and electron densities are reduced in the region occupied by the dust layer. It can be shown that a density $n_d \approx 10^2 \text{ cm}^{-3}$ of dust grains of diameter $2a \approx 100 \text{ nm}$ is sufficient to substantially reduce the mesospheric plasma density. These dust-grain parameters are common for NLC-type structures. It should be noted that a decrease in electron density reduces the loss of ions due to recombination. Therefore, while the presence of dust particles reduces the electron density, the ion density in the mesosphere may remain unchanged or even increase. These effects obviously depend on the relative importance of the ion losses due to recombination and collisions with dust grains. As the dust grain density exceeds a certain value, the equilibrium ion density becomes independent of the electron density and is controlled only by the loss of ions in collisions with dust particles, because the electron density is substantially reduced and the role played by ion losses due to recombination is insignificant. The left panels in Fig. 6 correspond to a dust particle material characterized by a relatively low work function ($W \approx 3$ to 4 eV). In this case, even if the dust particle density is low ($n_d \sim 10\text{-}100 \text{ cm}^{-3}$), the model [5] predicts an increase in electron density and a decrease in ion density, due to higher

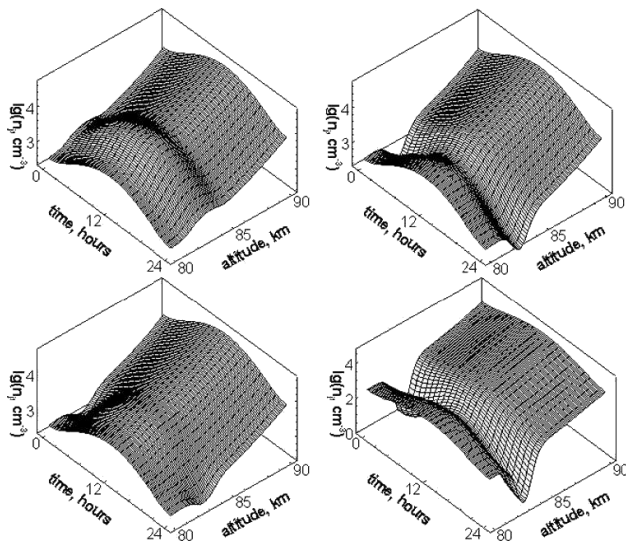


Fig. 6 Effect of the photoelectric properties of a dust layer on the electron and ion densities in the lower ionosphere. The right panels correspond to the absence of photoelectric emission from dust grains (the work function exceeds 7.3 eV, the cutoff of the solar spectrum at the mesospheric altitudes [12], as in the case of pure ice dust particles). The left panels illustrate strong effect of photoelectric emission on the plasma composition in the mesosphere (work function below 7.3 eV, as in the case of calcium dust particles). Top and bottom panels are electron and ion densities, respectively.

recombination losses.

Note that the mesospheric plasma exhibits a more diverse behavior when photoelectric emission plays a significant role. Depending on the dust particle size and density, virtually any effect due to the presence of dust particles in the mesosphere can be observed. Thus the model [5] can be used to predict the five trends (a)–(e) associated with NLC and PMSE enumerated above. The model [5] provides a unified explanation of these trends and of the presence of both positively and negatively charged particles in the upper atmosphere discovered by means of sounding rocket flights, as well as of the experimental fact that neither NLC nor PMSE can be observed permanently.

6. Some Other Examples

Applications of methods developed in studies of dusty plasma are also important for adequate description of such problems of Earth's sciences as active geophysical rocket experiments, formation of terrestrial planets, Schumann resonances, etc. Here, we outline the role of dusty plasma effects in these problems.

6.1 Active rocket experiments

The problem of interest is to investigate the possibility of an appearance of charged dust particles in active rocket experiments which involve the release of some gaseous

substance in near-Earth space. This can be reached using the scheme of the experiments analogous to that of the "Fluxus" and "North Star" experiments carried out in the ionosphere at altitudes of 140, 280, and 360 km [18–20]. The source for the charged particle release in the ionosphere in these experiments is the generator of high-speed plasma jets. Dust particles in the experiments appear as a result of condensation. The period of the formation of the centers of condensation is very short, and all drops have approximately the same size a [17, 48]. The formation of the dust particles in the active rocket experiments is confirmed by the results of both active and (modeling them) laboratory experiments as well as numerical simulations. In the first injection of the "North Star" experiment positively charged clusters of aluminium consisting of 2, 4, 8, and 16 atoms were detected in the jet [49]. The clusters of larger masses could not be detected because of the narrow range of the measured cluster energies. However the analysis [20] of electromagnetic radiation from the jet in the infra-red range of the spectrum shows the presence of micrometer-sized charged drops.

In [17] the idea has been forwarded of the formation of shocks related to dust charging in the active rocket experiments, which involve the release of some gaseous substance in near-Earth space. The shock wave front is associated with the fore (border)-part of the jet propagating in the plasma of the ionosphere. Drops appearing as a result of condensation are charged due to their interaction with the ambient plasma and the photoelectric effect. The optimum speeds of the jet are 10 km/s. The optimum altitudes for such experiments are 500–600 km. The scheme of the active experiment is given in Fig. 7. The active experiments, where the shocks in charge-varying dusty plasmas can be observed, can be helpful to model different physical phenomena occurring in nature, e.g., in the process of a large meteoroid impact with the Moon surface [50]. The evolution of the impact plume can lead to the formation of shock wave structure associated with an appearance of charged microparticles which are created in the process of condensation of the substance of vapor plume as well as are thrown from the crater and surrounding it regolith layer.

We emphasize that dusty plasma processes can occur in some other active geophysical experiments. For example, SEEK 2 experiment [51] conducted by JAXA with collaboration with a group of Clemson University shows very clear artificial optical emission that could be related to dusty plasma processes.

6.2 Primary Earth

Theory and the data of comparative planetology as well as the Earth sciences (consistent with each other) enable us to state that the formation of the terrestrial planets occurred during 30–100 million years beginning from an appearance of the first condensate approximately 4.6×10^9 years ago [52]. During the Earth growth the main energy

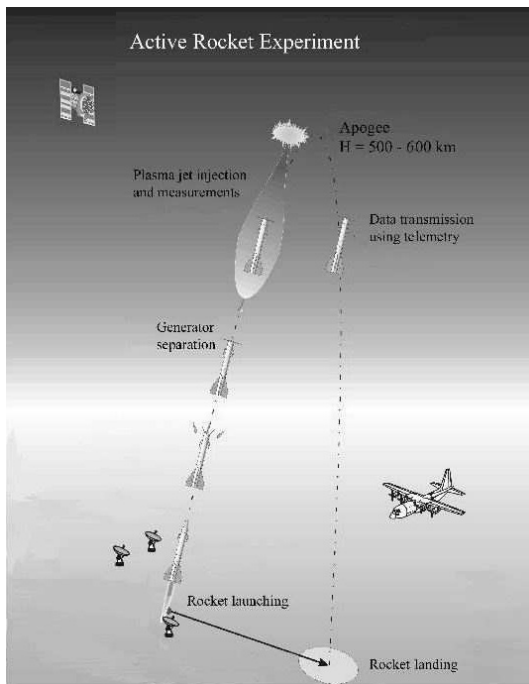


Fig. 7 The scheme of the active rocket experiment, which involves release of some gaseous substance in near-Earth space.

source was related to impacts of cosmic bodies falling to the growing planet. The mass spectrum of the cosmic bodies is considered to be proportional to m^{-q} , where $q \approx 1.8 \pm 0.2$. The main mass is concentrated in the bodies with diameters of 100 km and larger. Craters formed as a result of the impact of such large bodies with Earth's surface are estimated to have depths of the order of the Earth's diameter. The matter of the impact generated vapor plume has the mass of the order of the cosmic body (impacting the Earth) while its temperature reaches several electron-Volts. All this matter expands (lifts) with subsequent ionization, cooling, condensation, formation of nano- and microscale dust particles, and their charging. Thus the dusty plasma is formed. The important problem is to determine the characteristic sizes of the dust particles and estimate their mass spectrum because these will allow us to determine behavior of the dust grains: whether they work to the primary Earth's surface or they evolve in the primary atmosphere. This study will allow us to update the scenario of the formation of the primary Earth's crust, hydrosphere, and atmosphere and possibly to modify the scenario of the origin of terrestrial planets.

6.3 Schumann resonances (SRs)

SRs represent global electromagnetic oscillations excited by lightning discharges in a concentric spherical cavity formed by the Earth's surface and the lower ionosphere. As a rule, four or five first resonance peaks are recorded. The peak frequencies vary within several tenths of a hertz

near frequencies of about 8, 14, 20, and 26 Hz. The presence of dust grains in the Earth-ionosphere cavity can significantly enhance thunderstorm activity. Since this activity is directly related to the SR amplitude, an increase in the concentration of nano- and microscale particles in the atmosphere can raise the efficiency of energy pumping of the cavity [16]. For example, during violent volcanic eruptions, the SR amplitude can increase severalfold. The presence of dust particles in the atmosphere also influences the annual average temperature near the Earth's surface. For instance, violent volcanic eruptions are accompanied by an appreciable decrease in the annual average temperature. Since the SR amplitude is related to the surface temperature, a decrease in the temperature can lead to a decrease in the energy density in the cavity. Furthermore [16], the presence of dust particles in the lower ionosphere affects its dispersion properties, decreasing the frequencies and quality of the resonances.

7. Summary

Thus we have described possible observational manifestations of dusty ionospheric plasmas during high-speed meteor showers, namely, ground-based observations of low-frequency ionospheric radio noise with the frequencies lower than 50 Hz, ground-based observations of infrasonic waves, and amplification of the intensity of green emission at the wavelength of 557.7 nm from a layer of lower ionosphere located at 110-120 km. We have discussed physical processes accompanying formation of NLC and PMSE and presented a unified explanation of ionization properties of the polar mesosphere under summer conditions. Furthermore, we have considered dusty plasma processes in application to the description of active geophysical rocket experiments which involve release of some gaseous substance in near-Earth space, the origin of the primary Earth's crust, hydrosphere, and atmosphere, and the global electromagnetic Schumann resonances.

The author is grateful to the referee for valuable comments allowing the author to improve the manuscript. This study was supported by the Division of Earth Sciences, Russian Academy of Sciences (the basic research program "Nanoscale particles in nature and technogenic products: conditions of existence, physical and chemical properties, and mechanisms of formation") and by the Division of Physical Sciences, the Russian Academy of Sciences (the basic research program "Plasma physics in the solar system"). The author is also supported by the Dynasty Foundation.

- [1] V.E. Fortov, A.V. Ivlev, S.A. Khrapak, A.G. Khrapak and G.E. Morfill, *Phys. Rep.* **421**, 1 (2005).
- [2] K. Ostrikov, *Rev. Mod. Phys.* **77**, 489 (2005).
- [3] S.V. Vladimirov, K. Ostrikov and A.A. Samarian, *Physics and Applications of Complex Plasmas* (Imperial College Press, London, 2005).
- [4] F. Verheest, *Space Sci. Rev.* **68**, 109 (1994).

- [5] B.A. Klumov, G.E. Morfill and S.I. Popel, *Zh. Éksp. Teor. Fiz.* **127**, 171 (2005) [*JETP* **100**, 152 (2005)].
- [6] S.I. Popel and A.A. Gisko, *Nonlinear Proc. Geophys.* **13**, 223 (2006).
- [7] C. Anastasio and S.T. Martin, in *Nanoparticles and the Environment*, Ed. by J.F. Banfield and A. Navrotsky (Mineralogical Society of America, Washington DC, 2001) p. 293.
- [8] J.R. Holton, P.H. Haynes, M.E. McIntre, A.R. Douglass, R.B. Rood and L. Pfister, *Rev. Geophys.* **33**, 403 (1995).
- [9] D. Fromm and R. Servranckx, *Geophys. Rev. Lett.* **30**, 1542 (2003).
- [10] Yu.N. Besedina and S.I. Popel, *Doklady Akademii Nauk* **423**, 680 (2008) [*Doklady Earth Sciences* **423A**, 1475 (2008)].
- [11] M. Gadsen and W. Schröder, *Noctilucent Clouds* (Springer, Berlin, 1989).
- [12] B.A. Klumov, S.I. Popel and R. Bingham, *Pis'ma Zh. Éksp. Teor. Fiz.* **72**, 524 (2000) [*JETP Lett.* **72**, 364 (2000)].
- [13] O. Havnes, in *Dusty Plasma in the New Millennium*, Ed. by R. Bharuthram, M.A. Hellberg, P.K. Shukla and F. Verheest (AIP, New York, 2002) p. 13.
- [14] S.I. Kopnin, I.N. Kosarev, S.I. Popel and M.Y. Yu, *Planet. Space Sci.* **52**, 1187 (2004).
- [15] W.J. McNeil, *J. Geophys. Res.* **103**, 10899 (1998).
- [16] Yu.N. Besedina and S.I. Popel, *Fiz. Plazmy* **33**, 159 (2007) [*Plasma Phys. Rep.* **33**, 138 (2007)].
- [17] S.I. Popel and V.N. Tsytovich, *Astrophys. Space Sci.* **264**, 219 (1999).
- [18] B.G. Gavrilov, A.I. Podgorny, I.M. Podgorny, D.B. Sobyenin, J.I. Zetzer, R.E. Erlandson, C.-I. Meng and B.J. Stoyanov, *Geophys. Res. Lett.* **26**, 1549 (1999).
- [19] R.E. Erlandson, P.K. Swaminathan, C.-I. Meng, B.J. Stoyanov, J.I. Zetzer, B.G. Gavrilov, Yu.N. Kiselev and Yu.A. Romanovsky, *Geophys. Res. Lett.* **26**, 1553 (1999).
- [20] J.I. Zetzer, Yu.N. Kiselev, Yu.V. Poklad and V.A. Rybakov, in *Nano- and Microscale Particles in Geophysical Processes*, Ed. by V.V. Adushkin and S.I. Popel (MIPT, Moscow, 2006) p. 116 (in Russian).
- [21] V.N. Tsytovich and O. Havnes, *Comments Plasma Phys. Control. Fusion* **15**, 267 (1993).
- [22] N.N. Rao, P.K. Shukla and M.Y. Yu, *Planet. Space Sci.* **38**, 543 (1990).
- [23] S.I. Popel, M.Y. Yu and V.N. Tsytovich, *Phys. Plasmas* **3**, 4313 (1996).
- [24] S.I. Musatenko, Yu.S. Musatenko, E.V. Kurochka, M.M. Medvedskii, A.A. Sukhoi, A.S. Slipchenko and V.Ya. Choliij, *Geomagn. Aéron.* **41**, 812 (2001) [*Geomagn. Aeron.* **41**, 776 (2001)].
- [25] S.I. Musatenko, Yu.S. Musatenko, E.V. Kurochka, A.V. Lastochkin, V.Ya. Choliij, O.I. Maksimenko and A.S. Slipchenko, *Geomagn. Aéron.* **46**, 182 (2006) [*Geomagn. Aeron.* **46**, 173 (2006)].
- [26] S.I. Kopnin, S.I. Popel and M.Y. Yu, *Fiz. Plazmy* **33**, 323 (2007) [*Plasma Phys. Rep.* **33**, 289 (2007)].
- [27] S.I. Kopnin and S.I. Popel, in *New Vistas in Dusty Plasmas* (AIP, New York, 2005) p. 161.
- [28] S.V. Vladimirov, V.N. Tsytovich, S.I. Popel and F.Kh. Khakimov, *Modulational Interactions in Plasmas* (Kluwer, Dordrecht, 1995).
- [29] P.K. Shukla and S.V. Vladimirov, *Phys. Plasmas* **2**, 3179 (1995).
- [30] P.K. Shukla and L. Stenflo, *IEEE Trans. Plasma Sci.* **29**, 267 (2001).
- [31] S.I. Kopnin and S.I. Popel, *Fiz. Plazmy* **34**, 517 (2008) [*Plasma Phys. Rep.* **34**, 471 (2008)].
- [32] L.G. Evers and H.W. Haak, *Geophys. Rev. Lett.* **30**, 2246 (2003).
- [33] J.V. Olson, C.R. Wilson and R.A. Hansen, *Geophys. Rev. Lett.* **30**, 2195 (2003).
- [34] J.B. Johnson, R.C. Aster and P.R. Kyle, *Geophys. Rev. Lett.* **31**, L14604 (2004).
- [35] A. Le Pichon, V. Maurer, D. Raymond and O. Hyvernaud, *Geophys. Rev. Lett.* **31**, L19103 (2004).
- [36] M. Willis, M.A. Garces, C. Hetzer and S. Businger, *Geophys. Rev. Lett.* **31**, L19303 (2004).
- [37] L.D. Landau and E.M. Lifshitz, *Fluid Mechanics* (Pergamon, Oxford, 1987).
- [38] D.M. Hunten, R.P. Turco and O.B. Toon, *J. Atmosph. Sci.* **37**, 1342 (1980).
- [39] O. Havnes, T. Aslaksen and A. Brattli, *Phys. Scripta* **T89**, 133 (2001).
- [40] G.D. Aburdzhaniya, *Self-Organization of Vortex Structures and Vortex Turbulence in Dispersive Media* (KomKniga, Moscow, 2006) [in Russian].
- [41] G. Brasseur and S. Solomon, *Aeronomy of the Middle Atmosphere* (Reidel, Dordrecht, 1984).
- [42] Y. Chen, G. Wang and M.Y. Yu, *Planet. Space Sci.* **51**, 81 (2003).
- [43] J.X. Ma, Y. Chen, B. Gan and M.Y. Yu, *Planet. Space Sci.* **54**, 719 (2006).
- [44] J.Y.N. Cho and J. Röttger, *J. Geophys. Res.* **102**, 2001 (1997).
- [45] M. Rapp and F.J. Lübken, *J. Atmos. Sol.-Terr. Phys.* **63**, 759 (2001).
- [46] F. Balsiger, E. Kopp, M. Friedrich, K.M. Torkar, U. Walchli and G. Witt, *Geophys. Res. Lett.* **23**, 93 (1996).
- [47] F.F. Chen, in *Plasma Diagnostic Techniques*, Ed. by R.H. Huddleston and S.L. Leonard (Academic, New York, 1965) Chap. 4.
- [48] S.I. Popel, A.A. Gisko, A.P. Golub', T.V. Losseva, R. Bingham and P.K. Shukla, *Phys. Plasmas* **7**, 2410 (2000).
- [49] Yu.N. Kiselev, I.B. Kosarev and Yu.V. Poklad, in *Nano- and Microscale Particles in Geophysical Processes*, Ed. by V.V. Adushkin and S.I. Popel (MIPT, Moscow, 2006) p. 123 (in Russian).
- [50] I.V. Nemtchinov, V.V. Shuvalov, N.A. Artemieva, I.B. Kosarev and S.I. Popel, *Intern. J. Impact Engineering* **27**, 521 (2002).
- [51] M. Yamamoto, S. Fukao, R.T. Tsunoda, R. Pfaff and H. Hayakawa, *Annales Geophysicae* **23**, 2295 (2005).
- [52] A.V. Vitjazev, G.V. Pechernikova and V.S. Safronov, *Terrestrial Planets: Origin and Early Evolution* (Nauka, Moscow, 1990) [in Russian].